Geophysical Research Letters

Key Points:
- Wavelength dependence of permafrost dissolved organic carbon (DOC) photomineralization revealed a high lability to visible light
- Iron catalyzes the photomineralization of old permafrost DOC (>4,000 a BP) derived from soil lignin and tannin to carbon dioxide (CO_2)
- Photomineralization rates of permafrost DOC to CO_2 are double that of modern DOC, which will increase future arctic amplification

Supporting Information:
- Supporting Information S1

Correspondence to:
C. P. Ward and R. M. Cory,
cward@whoi.edu; rmcory@umich.edu

Arctic Amplification of Global Warming Strengthened by Sunlight Oxidation of Permafrost Carbon to CO_2

J. C. Bowen[1] , **C. P. Ward[2]** , **G. W. Kling[3]** , and **R. M. Cory[1]**

[1]Department of Earth and Environmental Sciences, University of Michigan, Ann Arbor, MI, USA, [2]Department of Marine Chemistry and Geochemistry, Woods Hole Oceanographic Institution, Woods Hole, MA, USA, [3]Department of Ecology and Evolutionary Biology, University of Michigan, Ann Arbor, MI, USA

Abstract Once thawed, up to 15% of the ~1,000 Pg of organic carbon (C) in arctic permafrost soils may be oxidized to carbon dioxide (CO_2) by 2,100, amplifying climate change. However, predictions of this amplification strength ignore the oxidation of permafrost C to CO_2 in surface waters (photomineralization). We characterized the wavelength dependence of permafrost dissolved organic carbon (DOC) photomineralization and demonstrate that iron catalyzes photomineralization of old DOC (4,000–6,300 a BP) derived from soil lignin and tannin. Rates of CO_2 production from photomineralization of permafrost DOC are twofold higher than for modern DOC. Given that model predictions of future net loss of ecosystem C from thawing permafrost do not include the loss of CO_2 to the atmosphere from DOC photomineralization, current predictions of an average of 208 Pg C loss by 2,299 may be too low by ~14%.

Plain Language Summary The thawing of organic carbon stored in arctic permafrost soils, and its oxidation to carbon dioxide (a greenhouse gas), is predicted to be a major, positive feedback on global warming. However, current estimates of the magnitude of this feedback do not include the oxidation of permafrost soil organic carbon flushed to sunlit lakes and rivers. Here we show that ancient dissolved organic carbon (>4,000 years old) draining permafrost soils is readily oxidized to carbon dioxide by sunlight. As a consequence, current estimates of additional global warming from the permafrost carbon feedback are too low.

1. Introduction

Current estimates are that 5% to 15% of the ~1,000 Pg of the soil organic carbon (C) stored in surface permafrost soils could be emitted as greenhouse gases by 2,100 given the current trajectory of global warming (Plaza et al., 2019; Schuur et al., 2015), with additional C lost in lateral transfer from soils to surface waters (Plaza et al., 2019). Models assessing the sensitivity of the climate system to thawing permafrost soils estimate that decomposition of organic C in these soils could result in 0.3°C to 0.4°C additional global warming (i.e., arctic amplification) by 2,100 to 2,299, respectively (McGuire et al., 2018). However, none of these predictions include the oxidation of organic C upon export to sunlit surface waters.

Oxidation of dissolved organic carbon (DOC) to carbon dioxide (CO_2) by sunlight (photomineralization) currently accounts for up to 30% of the CO_2 emitted to the atmosphere from arctic surface waters (Cory et al., 2014). As permafrost DOC is exported to sunlit waters, its oxidation to CO_2 will depend on whether permafrost DOC is labile to photomineralization, which is currently debated (Selvam et al., 2017; Shirokova et al., 2019; Stubbins et al., 2016; Ward & Cory, 2016). The lability of terrestrially derived DOC to photomineralization is hypothesized to depend on iron and DOC chemical composition (Gao & Zepp, 1998; Gu et al., 2017; Miles & Brezonik, 1981; Ward & Cory, 2016; Xie et al., 2004). To test these hypothesized controls, we made the first direct measurements of the amount, source, and age of CO_2 produced from photomineralization of permafrost DOC collected on younger and older glacial surfaces, and from two common vegetation types in the Arctic (Table S1; Ping et al., 1998; Trusiak et al., 2019). Here we show that (i) the lability of permafrost DOC to photomineralization depends on sunlight wavelength, (ii) iron controls the lability of permafrost DOC to photomineralization, and (iii) old carboxylic acid C (4,000 to 6,300 a BP) derived from lignin and tannin is mineralized to CO_2 by sunlight. Collectively, our results support the inclusion of photomineralization in model predictions and experimental studies of arctic amplification of climate change.

2. Methods

2.1. Permafrost Soil Collection

Soils were collected from the frozen permafrost layer (>60 cm below the surface) at five sites underlying moist acidic tussock or wet sedge vegetation, and on three glacial surfaces on the North Slope of Alaska during summer 2018 (Table S1; Hobbie & Kling, 2014; Mull & Adams, 1989; Walker et al., 2005). See the Supporting Information for soil collection protocols, including precautions to minimize radiocarbon (^{14}C) contamination, and for a summary of the experimental design. DOC was leached from each permafrost soil (leachate) at the Woods Hole Oceanographic Institution (WHOI) as described in the Supporting Information.

2.2. Δ^{14}C and δ^{13}C Analyses of DOC

The ^{14}C and stable carbon (^{13}C) isotopic compositions of DOC were analyzed from each permafrost leachate at the National Ocean Sciences Accelerator Mass Spectrometry (NOSAMS) facility at WHOI (Table S2) following Beaupré et al. (2007). Each permafrost leachate was diluted with UVC-oxidized MilliQ water (Millipore Simplicity ultraviolet, UV, system; 1.5 hr; 1,200-W medium pressure mercury arc lamp) to achieve a total C mass between 800 and 2,000 μg. The diluted permafrost leachate was acidified with UVC-oxidized trace-metal grade phosphoric acid (85%) to pH < 2 in a precombusted quartz reactor (450°C; 4 hr), and the dissolved inorganic carbon (DIC) was purged with high-purity helium gas in the dark. The DOC was then oxidized with UVC light to DIC for 4 hr (1,200-W medium pressure mercury arc lamp), and the resultant CO_2 was extracted cryogenically. On average, $1,370 \pm 240$ μg of C were extracted from each permafrost leachate (± 1 standard error, SE; $n = 6$; Table S2). A subsample of the CO_2 was analyzed for ^{13}C using a VG Prism-II or Optima stable isotope ratio mass spectrometer (instrumental precision of 0.1‰; Coplen et al., 2006), and the δ^{13}C (‰) was calculated as follows:

$$\delta^{13}C = \left(^{13}R_{\text{sample}}/^{13}R_{\text{standard}} - 1\right), \tag{1}$$

where ^{13}R is the isotope ratio of a sample or standard (VPDB), as defined by

$$^{13}R = \left(^{13}C/^{12}C\right). \tag{2}$$

The remaining CO_2 was reduced to graphite with H_2 and an iron catalyst, and then analyzed for ^{14}C isotopic composition using an accelerator mass spectrometer at the NOSAMS facility (Longworth et al., 2015). The Δ^{14}C (‰) and radiocarbon age of DOC were calculated from the fraction modern (McNichol et al., 2001; Stuiver & Polach, 1977) using the oxalic acid I standard (NIST-SRM 4990). Δ^{14}C analyses of DOC had an instrumental precision of 2–6‰ (Longworth et al., 2015; McNichol et al., 2001).

DOC leached from one permafrost soil (Toolik moist acidic tundra) was prepared and analyzed for ^{14}C and ^{13}C twice to quantify the standard error of duplicate analyses (Table S2). Δ^{14}C and δ^{13}C analyses of DOC had standard errors of 1‰ and 0.1‰, respectively (1 SE; $n = 2$; Table 1). A procedural blank was quantified manometrically by oxidizing MilliQ water with UVC light in a precombusted quartz reactor (450°C; 4 hr) for 1.5 hr, acidifying to pH < 2, and purging the DIC as described above. The procedural blank was 4 μg of C, which was <0.5% of the total C masses extracted from the permafrost leachates.

2.3. Apparent Quantum Yield Spectra

The CO_2 produced from photomineralization of permafrost DOC was measured as a function of sunlight wavelength. The lability of DOC to photomineralization is defined as the apparent quantum yield spectrum (CO_2 produced per mol photon absorbed by DOC; hereafter called the yield spectrum, $\varphi_{\text{PM},\lambda}$). Yield spectra of permafrost DOC were directly measured for the first time with a custom-built high-powered ($\geq$100 mW), narrow-banded ($\pm$10 nm) light-emitting diode (LED) system from soils collected in 2018 (Figure S1). Each permafrost leachate was equilibrated to room temperature (~24 hr) and then placed in 20 gas-tight, flat-bottomed precombusted (450°C; 4 hr) 12-mL quartz vials with butyl rubber septa and GL-18 caps (light-exposed vials) and four gas-tight precombusted (450°C; 4 hr) 12-mL borosilicate exetainer vials (dark control vials; Labco, Inc.). Vials were placed in an inner aluminum housing (painted black matte to minimize light scattering), with the flat bottom facing upward toward the light source, and then exposed to

Table 1
$\Delta^{14}C$ and $\delta^{13}C$ of Initial, Bulk Permafrost DOC and the CO_2 Produced by UV and Visible Light

	Light source	Toolik moist acidic tundra	Imnavait moist acidic tundra	Imnavait wet sedge tundra	Sagwon wet sedge tundra	Sagwon moist acidic tundra
$\Delta^{14}C$-DOC (‰)		-436 ± 1	-474	-585	-411	-519
^{14}C age of DOC (a BP)		$4{,}520 \pm 5$	$5{,}080$	$6{,}990$	$4{,}300$	$5{,}890$
$\delta^{13}C$-DOC (‰)		-25.5 ± 0.1	-25.4	-26.1	-27.8	-26.9
$\Delta^{14}C$-CO_2 produced (‰)	UV	-487 ± 4	-465 ± 8	-546 ± 11	-397 ± 1	N/A
	Visible	-506	-454 ± 8	-538 ± 13	-402	N/A
^{14}C age of CO_2 produced (a BP)	UV	$5{,}300 \pm 55$	$4{,}950 \pm 110$	$6{,}270 \pm 190$	$4{,}000 \pm 5$	N/A
	Visible	$5{,}600$	$4{,}800 \pm 120$	$6{,}150 \pm 220$	$4{,}070$	N/A
$\delta^{13}C$-CO_2 produced (‰)	UV	-30.2 ± 0.4	-31.0 ± 0.4	-31.8 ± 1.8	-35.8 ± 0.6	N/A
	Visible	-29.8	-28.3 ± 0.4	-29.2 ± 2.0	-36.0	N/A

Note. The $\Delta^{14}C$ and $\delta^{13}C$ of the CO_2 produced from photomineralization of permafrost DOC are reported following exposure to LEDs at 309 (UV) or 406 nm (visible). When available, all values are reported as the average $\pm$ 1 SE of experimental replicates ($n = 2$).

$\geq$100-mW, narrow-banded ($\pm$10 nm) LEDs at 278, 309, 348, 369, and 406 nm alongside the dark controls for 12 or 30 hr (Table S3). The LEDs were tuned such that each permafrost leachate absorbed the same amount of light at each wavelength. After LED exposure, light-exposed and dark control waters were immediately analyzed for DIC (Apollo SciTech, Inc.) and for chromophoric dissolved organic matter (CDOM; Cory et al., 2014). The experiment above was then repeated for the analysis of photochemical oxygen (O_2) consumption to quantify the apparent quantum yield spectra of photo-oxidation ($\varphi_{PO,\lambda}$) from each permafrost DOC. Dissolved O_2 was measured in each light-exposed and dark control vial on a membrane inlet mass spectrometer (Bay Instruments; Kana et al., 1994).

At each LED wavelength, $\varphi_{PM,\lambda}$ and $\varphi_{PO,\lambda}$ were calculated as the concentration of DIC produced and O_2 consumed, respectively, divided by the light absorbed by CDOM. The amount of light absorbed by CDOM (mol photon m^{-2} nm^{-1}) was quantified for each vial exposed to a LED using absorption coefficients of CDOM ($a_{CDOM,\lambda}$) and the photon flux spectrum (Cory et al., 2014). The photon flux spectrum was quantified from the solar irradiance spectrum from each LED source, which was measured by radiometry and chemical actinometry (see the Supporting Information). $\varphi_{PM,\lambda}$ and $\varphi_{PO,\lambda}$ are reported as the average $\pm$ 1 SE of experimental replicate vials ($n = 4$).

2.4. $\Delta^{14}C$ and $\delta^{13}C$ of CO_2 Produced From Light

The $\Delta^{14}C$ and $\delta^{13}C$ of DIC produced following exposure of DOC to UV and visible light were quantified from permafrost leachates prepared from each permafrost soil collected in 2018, except for Sagwon moist acidic tundra (Figure S1). Each permafrost leachate was equilibrated to room temperature and then placed in up to four precombusted (450°C; 4 hr) 600-mL quartz flasks with ground glass stoppers and no headspace. The flasks were exposed to custom-built LED arrays consisting of ten $\geq$100 mW, narrow-banded ($\pm$10 nm) 309- or 406-nm chips alongside one or two foil-wrapped dark control flasks (Table S2). Exposure times ranged from 8 to 25 hr to achieve similar concentrations of DIC produced from each permafrost DOC sample and at each wavelength (Table S4).

After LED exposure, foil-wrapped light-exposed and dark control flasks were immediately transferred to foil-wrapped, precombusted 500-mL borosilicate glass bottles (450°C; 4 hr) in a N_2-filled glove bag, preserved with saturated mercuric chloride, and plugged with gas-tight ground glass stoppers (McNichol et al., 1994). Those bottles were stored in the dark at room temperature for $\leq$1 week until preparation for carbon isotope analyses at the NOSAMS facility. Bottles were kept foil-wrapped while each water sample was acidified with trace-metal grade phosphoric acid (85%) to pH < 2 and stripped of DIC with high-purity N_2 gas. The resultant CO_2 was trapped and purified cryogenically and its concentration was quantified manometrically. The ^{14}C and ^{13}C of the CO_2 were analyzed at the NOSAMS facility (Table S2) and converted to $\Delta^{14}C$ and $\delta^{13}C$ values as described above. $\Delta^{14}C$ analyses of DIC had an instrumental precision of 1–2‰ (Longworth et al., 2015; McNichol et al., 2001). The reported precision of $\delta^{13}C$ is 0.1‰ (Coplen et al., 2006).

The $\Delta^{14}C$ and $\delta^{13}C$ of CO_2 produced from the photomineralization of DOC were calculated as follows:
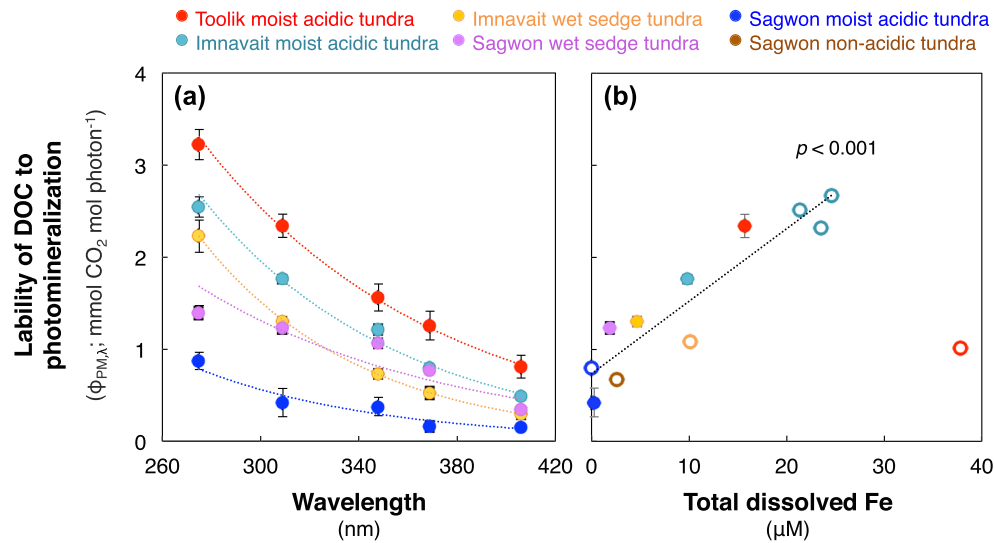
Figure 1. Controls on the lability of permafrost DOC to photomineralization. (a) Wavelength-dependent apparent quantum yield spectrum for photomineralization ($\varphi_{PM,\lambda}$) of permafrost DOC. Each data series was fit with a least-squares exponential model where $R^2 > 0.83$, $p < 0.05$. (b) Apparent quantum yield for photomineralization at 309 nm ($\varphi_{PM,309}$) versus total dissolved iron concentration in permafrost leachates prior to light exposure. Closed symbols indicate $\varphi_{PM,309}$ measured following LED exposure at 309 nm. Open symbols indicate $\varphi_{PM,309}$ estimated from an exponential fit following exposure to broadband light (see section 2). Data in panel (b) were fit using a least-squares regression where $R^2 = 0.87$, t statistic $= 7.8$, $p < 0.001$, excluding the open red symbol (see the Supporting Information). Open symbols for Imnavait moist acidic tundra were previously reported (Ward & Cory, 2016). All values are the average ± 1 SE of experimental replicates ($n = 2$ and 4 for open and closed symbols, respectively; see section 2). $\varphi_{PM,\lambda}$ at other wavelengths versus dissolved iron are reported in the Supporting Information.

$$\Delta^{14}\text{C}-\text{CO}_{2\lambda} = \frac{\left(\Delta^{14}\text{C} - \text{DIC}_{\text{Light},\lambda}*[\text{DIC}]_{\text{Light},\lambda}\right) - \left(\Delta^{14}\text{C} - \text{DIC}_{\text{Dark}}*[\text{DIC}]_{\text{Dark}}\right)}{\left([\text{DIC}]_{\text{Light},\lambda} - [\text{DIC}]_{\text{Dark}}\right)}, \tag{3}$$

$$\delta^{13}\text{C}-\text{CO}_{2\lambda} = \frac{\left(\delta^{13}\text{C} - \text{DIC}_{\text{Light},\lambda}*[\text{DIC}]_{\text{Light},\lambda}\right) - \left(\delta^{13}\text{C} - \text{DIC}_{\text{Dark}}*[\text{DIC}]_{\text{Dark}}\right)}{\left([\text{DIC}]_{\text{Light},\lambda} - [\text{DIC}]_{\text{Dark}}\right)}. \tag{4}$$

The Δ^{14}C and δ^{13}C of CO_2 produced in each light-exposed flask were calculated relative to one or two dark controls (Tables S2 and S4) and are reported as the average ± 1 SE of replicate values for the experiments conducted alongside two dark controls (Table 1). The concentration, Δ^{14}C, and δ^{13}C of DIC in the dark controls are reported as the average ± 1 SE of replicate flasks ($n = 2$; Table S4). The ^{14}C age of CO_2 produced is the age of DIC in light-exposed flask minus the ^{14}C age of DIC in the dark control (Table 1). This approach to quantify the Δ^{14}C and δ^{13}C of CO_2 produced from photomineralization of organic C was previously described in detail for polystyrene (Ward et al., 2019). In this previous study, experimental reproducibility of Δ^{14}C and δ^{13}C of CO_2 produced from photomineralization was 5‰ and 0.1‰, respectively (± 1 SE; $n = 3$).

3. Results and Discussion

All permafrost DOC was labile to photomineralization at all wavelengths measured (Figure 1a), and the yield spectrum always decreased exponentially with increasing wavelength from the UV to the visible ($p < 0.05$; Figure 1a). The magnitude of the photomineralization yield varied up to eightfold among permafrost DOC samples (Figure 1a) and was significantly, positively correlated with the concentration of dissolved iron ($p < 0.001$ as shown at 309 nm in Figure 1b; see the Supporting Information). There were no significant correlations of the photomineralization yield with dissolved cations other than iron or with any measure of DOC concentration or composition (see the Supporting Information).

Our results are the first to demonstrate in natural samples that the lability of permafrost DOC to photomineralization is controlled by dissolved iron. Although photomineralization of terrestrially derived DOC has
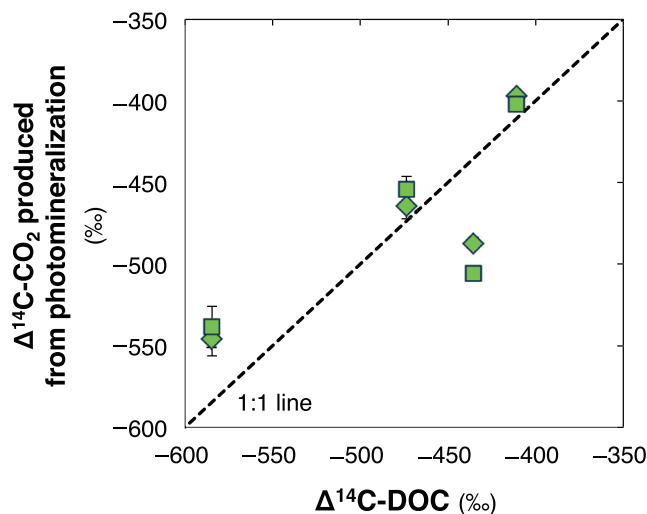
Figure 2. Δ^{14}C of bulk permafrost DOC was a strong predictor of the Δ^{14}C-CO_2 produced from photomineralization of DOC. Δ^{14}C-CO_2 produced from exposure of permafrost DOC to UV (309 nm, diamond symbols) and visible (406 nm, square symbols) light versus Δ^{14}C of initial, bulk permafrost DOC plotted with the 1:1 line. When all data are fit using a least-squares regression, $R^2 = 0.66$, t statistic = 3.4, $p < 0.05$. Values for photochemically produced Δ^{14}C-CO_2 are shown as the average $\pm$ 1 SE of experimental replicates ($n = 2$).

been shown to increase with addition or decrease with removal of iron in the laboratory (Gao & Zepp, 1998; Gu et al., 2017; Miles & Brezonik, 1981; Xie et al., 2004), evidence is lacking for a mechanism by which iron enhances photomineralization. Here we present new experimental evidence and a synthesis of literature results that collectively support a mechanism of iron-catalyzed photo-decarboxylation of lignin- and tannin-derived carboxylic acids within old permafrost DOC.

Iron is hypothesized to catalyze the photo-decarboxylation of organic acids by a ligand-metal-charge-transfer reaction (Mangiante et al., 2017) where Fe(III) is a cyclic catalyst that is photo-reduced to Fe(II) while the C in carboxylic acids (hereafter "carboxyl C") is oxidized to CO_2 (Gao & Zepp, 1998; Miles & Brezonik, 1981; Xie et al., 2004). Two lines of evidence from our study strongly support iron-catalyzed photo-decarboxylation of permafrost DOC to CO_2. First, loss of carboxyl C (quantified by ^{13}C nuclear magnetic resonance) upon exposure of permafrost DOC to sunlight was significantly, positively correlated with the dissolved iron concentration ($p < 0.05$; Figure S2), as expected if photo-decarboxylation is the mechanism of CO_2 production. The only other study that quantified photochemical loss of carboxyl C from permafrost DOC concluded that it accounted for up to 90% of the CO_2 produced from photomineralization (Ward & Cory, 2016). However, this prior study used DOC from one site (with only one iron concentration) and thus was unable to link iron abundance to DOC photo-decarboxylation. Second, the ratio of photochemical CO_2 production per dissolved O_2 consumption by DOC was ≥ 1 for all permafrost DOC that also contained >1-μM total dissolved iron (Figure S3). A ratio ≥ 1 for photochemical CO_2 produced per O_2 consumed is considered evidence for photo-decarboxylation because this reaction is expected to proceed with a stoichiometry of $\geq 2{:}1$ mol CO_2 produced per mol O_2 consumed (Miles & Brezonik, 1981; Xie et al., 2004). While ratios ≥ 1 for photochemical CO_2 produced per O_2 consumed have previously been observed in high-iron waters (Cory et al., 2015; Miles & Brezonik, 1981; Xie et al., 2004), here we show ratios ≥ 1 for DOC from various permafrost soils concurrent with photochemical loss of carboxyl C.

Isotopic signatures of the CO_2 produced by sunlight indicate that iron is catalyzing the oxidation of carboxyl C attached to organic matter derived from lignin and tannin. Photochemical production of ^{13}C-depleted CO_2 (Table 1) increased significantly with the ratio of photochemical CO_2 produced per mol of O_2 consumed ($p < 0.05$; Figure S4). Therefore, as photo-decarboxylation accounts for more of the total CO_2 produced (as indicated by increasing CO_2/O_2; Figure S4), the source of the CO_2 is increasingly ^{13}C-depleted carboxyl C, such as that derived from lignin and tannin (Ball & Aluwihare, 2014). Photochemical production of ^{13}C-depleted CO_2 is interpreted as resulting from photomineralization of lignin- or tannin-derived DOC (Franke et al., 2012; Spencer et al., 2009) because lignin and tannin are relatively more depleted in ^{13}C compared to other fractions of DOC (Benner et al., 1987; see the Supporting Information). In addition, the ^{13}C enrichment of DOC remaining after photomineralization has been correlated with photochemical loss of lignin (Spencer et al., 2009), and high-resolution mass spectrometry revealed that lignin- and tannin-derived compounds within permafrost DOC are preferentially degraded by sunlight compared to other fractions of DOC (Ward et al., 2017; Ward & Cory, 2016). Thus, our results indicate that iron-catalyzed photo-decarboxylation of lignin and tannin in permafrost DOC is producing CO_2 (Table 1, Figures S2 and S4).

The carboxyl C derived from lignin and tannin that was photomineralized to CO_2 was old, from 4,000 to 6,300 a BP (Table 1, Figure 2). The Δ^{14}C composition of CO_2 produced from photomineralization of permafrost DOC (−546‰ to −397‰) was always ≤70‰ different from the initial, bulk Δ^{14}C-DOC signature (−585‰ to −411‰; Table 1, Figure 2). The linear relationship between the initial, bulk permafrost Δ^{14}C-DOC and the Δ^{14}C-CO_2 produced by photomineralization ($p < 0.05$; Figure 2) indicates that the bulk age of permafrost DOC was a strong predictor of the age of DOC photomineralized to CO_2. Collectively, our
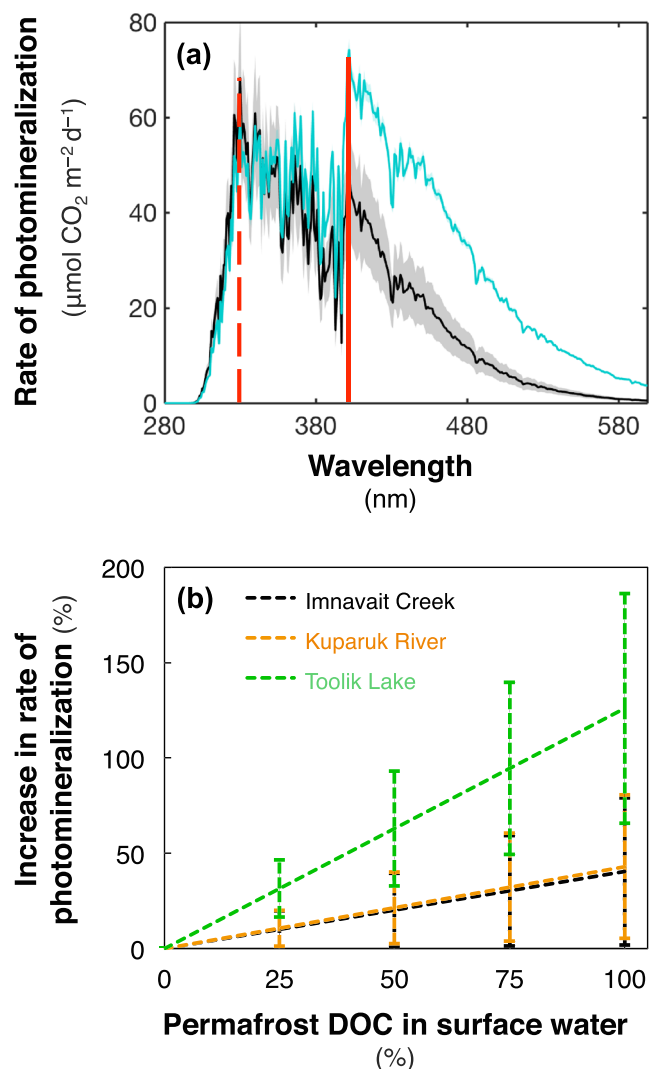
Figure 3. Photomineralization rates were higher for permafrost DOC than for surface water DOC due to higher lability in the visible light region. (a) Wavelength-dependent water column rates of photomineralization for Imnavait moist acidic tundra permafrost DOC and Imnavait Creek DOC (turquoise vs. black line, respectively). Solid lines show the average photomineralization rate spectrum and the similar color shading shows the upper and lower 95% confidence intervals. Rates of photomineralization were calculated using the different wavelength-dependent apparent quantum yields for photomineralization ($\varphi_{PM,\lambda}$) for Imnavait moist acidic tundra permafrost DOC or Imnavait Creek DOC (Figure S5; see the Supporting Information). The red dashed and solid lines mark the wavelength of peak photomineralization rates (330 nm vs. 402 nm) for Imnavait Creek and Imnavait moist acidic tundra permafrost DOC, respectively. (b) Calculated photomineralization rates increased with an increasing fraction of permafrost DOC in the surface water DOC pool. Percent increase in photomineralization rates as permafrost DOC comprises 0–100% of the DOC pool in Imnavait Creek, Kuparuk River, and Toolik Lake (compared to no permafrost DOC in the DOC pool). Only the $\varphi_{PM,\lambda}$ was varied in the water column rate calculations, using a "mixed" $\varphi_{PM,\lambda}$ calculated as a mixture of the $\varphi_{PM,\lambda}$ for permafrost DOC with the $\varphi_{PM,\lambda}$ for the surface water DOC (see the Supporting Information). All values are shown as the average $\pm$ 1 SE of calculated rates for surface water DOC mixed with each of the five permafrost DOCs in this study ($n = 5$).

results demonstrate that old carboxyl C (4,000 to 6,300 a BP) derived from lignin and tannin and associated with iron is photomineralized to CO_2.

The presence of iron may explain contrasting literature results from high (Selvam et al., 2017; Shirokova et al., 2019; Ward & Cory, 2016) to little or no (Shirokova et al., 2019; Stubbins et al., 2016) lability of permafrost DOC to photomineralization. For example, undetectable photomineralization of permafrost DOC from Russian arctic thaw slumps (Stubbins et al., 2016) may have been due to the 100-fold dilution of the DOC with deionized water. Although dissolved iron was not reported (Stubbins et al., 2016), dilution likely also resulted in the precipitation of iron (oxy)hydroxides and thus lower dissolved iron concentrations (Miller et al., 2009). In a study of Russian arctic surface waters that likely contained permafrost DOC (Shirokova et al., 2019), up to 13% of the DOC pool was photomineralized to CO_2, consistent with the presence of dissolved iron (3–7 μM). Provided that all permafrost DOC contains carboxyl C (Feng et al., 2017; Ward et al., 2017; Ward & Cory, 2016) and that permafrost soils generally contain high levels of leachable iron (Herndon et al., 2015; Heslop et al., 2019; Ping et al., 1998; Trusiak et al., 2019), arctic permafrost DOC is labile to photomineralization in proportion to the iron present. Given that the export of iron is currently strongly, positively correlated with DOC export from arctic soils to surface waters (Trusiak et al., 2019), we expect that iron and DOC export may continue to covary as permafrost soils thaw. Therefore, we predict that the yield spectrum of permafrost DOC will be within the range reported here in the future (Figure 1a).

The photomineralization yield spectra of permafrost DOC directly measured in this study have significantly shallower spectral slopes compared to those quantified indirectly for arctic surface water DOC (two-tailed, unpaired t test; $p < 0.001$; Figure S5). Thus, permafrost DOC has relatively lower lability to photomineralization at UV wavelengths and higher lability at visible wavelengths (different at 95% confidence interval; Figure S5). If permafrost DOC comprises 100% of the DOC in surface water, photomineralization rates will increase by twofold compared to current rates (Figure 3a) due to the higher lability of permafrost DOC at visible wavelengths multiplied by the approximately tenfold greater photon flux in the visible versus the UV light region (Table S5). It follows that photomineralization rates increase in proportion to the permafrost DOC exported to surface waters (Figure 3b).

4. Implications

The uncertainty in model predictions of future ecosystem C gain or loss crosses zero (McGuire et al., 2018). For example, under the RCP8.5 scenario, a net ecosystem loss of C of 208 $\pm$ 307 Pg C is predicted by 2,299 (average $\pm$ 1 SD). The large uncertainty in model predictions of permafrost C storage in this scenario includes a 20% probability that the net C storage is between +100 (gain) or −100 (loss) Pg C (see the Supporting Information). Photomineralization of DOC to CO_2 is always a loss to the atmosphere, and as the net C gain or loss for any particular year or over time nears zero, the relative importance of photomineralization increases. Given that photomineralization rates of permafrost DOC are nearly twofold higher than for modern DOC in arctic surface waters (Figure 3a), and assuming from 2,010 to 2,299 that 75% of DOC in surface waters was delivered from permafrost soils, then the photomineralization rates

of 20 g C m^{-2} y^{-1} reported in Cory et al. (2014) would increase to 39 g C m^{-2} y^{-1}. Using a surface area of water in permafrost regions of 6% (Cooley et al., 2019), ~9 Pg CO_2 could be produced from the photomineralization of permafrost DOC by 2,299 (see the Supporting Information). In addition, if potentially more than half of future terrestrial C losses are lateral in hydrologic flow (Plaza et al., 2019), a pathway missing from models used in McGuire et al. (2018), photomineralization of that C would occur upon exposure to sunlight. For example, taking the predicted net ecosystem loss of 208 Pg C by 2,299 under RCP8.5 (McGuire et al., 2018), potentially another ~100 Pg C could be lost laterally and produce ~21 Pg C as CO_2 from photomineralization in surface waters (Cory et al., 2014; see the Supporting Information). CO_2 from photodegradation of permafrost DOC is conservative because it does not account for (a) increased lability of permafrost DOC to microbial respiration following exposure to sunlight (Cory et al., 2013; Ward et al., 2017) and (b) increased annual sunlight exposure due to more ice-free days for surface waters in a warmer Arctic (Šmejkalová et al., 2016). Therefore, reducing the uncertainty on whether permafrost thaw will be a net sink or source of C to the atmosphere requires representing processes such as photochemistry in models of the future arctic C balance.

Data Availability Statement

All data are available in the manuscript or the Supporting Information, and data are available at the Arctic LTER (https://arc-lter.ecosystems.mbl.edu/arctic-coupled-biological-and-photochemical-degradation-dissolved-organic-carbon/data-photo-coupled).

Conflict of Interest

The authors declare no competing financial interests.

References

Ball, G. I., & Aluwihare, L. I. (2014). CuO-oxidized dissolved organic matter (DOM) investigated with comprehensive two dimensional gas chromatography-time of flight-mass spectrometry (GC × GC-TOF-MS). *Organic Geochemistry*, *75*, 87–98. https://doi.org/10.1016/j.orggeochem.2014.06.010

Beaupré, S. R., Druffel, E. R. M., & Griffin, S. (2007). A low-blank photochemical extraction system for concentration and isotopic analyses of marine dissolved organic carbon. *Limnology and Oceanography: Methods*, *5*(6), 174–184. https://doi.org/10.4319/lom.2007.5.174

Benner, R., Fogel, M. L., Sprague, E. K., & Hodson, R. E. (1987). Depletion of ^{13}C in lignin and its implications for stable carbon isotope studies. *Nature*, *329*(6141), 708–710. https://doi.org/10.1038/329708a0

Cooley, S. W., Smith, L. C., Ryan, J. C., Pitcher, L. H., & Pavelsky, T. M. (2019). Arctic-boreal lake dynamics revealed using CubeSat imagery. *Geophysical Research Letters*, *46*, 2111–2120. https://doi.org/10.1029/2018GL081584

Coplen, T. B., Brand, W. A., Gehre, M., Gröning, M., Meijer, H. A. J., Toman, B., & Verkouteren, R. M. (2006). New guidelines for δ^{13}C measurements. *Analytical Chemistry*, *78*(7), 2439–2441. https://doi.org/10.1021/ac052027c

Cory, R. M., Crump, B. C., Dobkowski, J. A., & Kling, G. W. (2013). Surface exposure to sunlight stimulates CO_2 release from permafrost soil carbon in the Arctic. *Proceedings of the National Academy of Sciences of the United States of America*, *110*(9), 3429–3434. https://doi.org/10.1073/pnas.1214104110

Cory, R. M., Harrold, K. H., Neilson, B. T., & Kling, G. W. (2015). Controls on dissolved organic matter (DOM) degradation in a headwater stream: The influence of photochemical and hydrological conditions in determining light-limitation or substrate-limitation of photo-degradation. *Biogeosciences*, *12*(22), 6669–6685. https://doi.org/10.5194/bg-12-6669-2015

Cory, R. M., Ward, C. P., Crump, B. C., & Kling, G. W. (2014). Sunlight controls water column processing of carbon in arctic fresh waters. *Science*, *345*(6199), 925–928. https://doi.org/10.1126/science.1253119

Feng, X., Vonk, J. E., Griffin, C., Zimov, N., Montluçon, D. B., Wacker, L., & Eglinton, T. I. (2017). ^{14}C variation of dissolved lignin in arctic river systems. *ACS Earth Space Chem.*, *1*(6), 334–344. https://doi.org/10.1021/acsearthspacechem.7b00055

Franke, D., Hamilton, M. W., & Ziegler, S. E. (2012). Variation in the photochemical lability of dissolved organic matter in a large boreal watershed. *Aquatic Sciences*, *74*(4), 751–768. https://doi.org/10.1007/s00027-012-0258-3

Gao, H., & Zepp, R. G. (1998). Factors influencing photoreactions of dissolved organic matter in a coastal river of the southeastern United States. *Environmental Science & Technology*, *32*(19), 2940–2946. https://doi.org/10.1021/es9803660

Gu, Y., Lensu, A., Perämäki, S., Ojala, A., & Vähätalo, A. V. (2017). Iron and pH regulating the photochemical mineralization of dissolved organic carbon. *ACS Omega*, *2*(5), 1905–1914. https://doi.org/10.1021/acsomega.7b00453

Herndon, E. M., Yang, Z., Bargar, J., Janot, N., Regier, T. Z., Graham, D. E., et al. (2015). Geochemical drivers of organic matter decomposition in arctic tundra soils. *Biogeochemistry*, *126*(3), 397–414. https://doi.org/10.1007/s10533-015-0165-5

Heslop, J. K., Winkel, M., Walter Anthony, K. M., Spencer, R. G. M., Podgorski, D. C., Zito, P., et al. (2019). Increasing organic carbon biolability with depth in yedoma permafrost: Ramifications for future climate change. *Journal of Geophysical Research: Biogeosciences*, *124*, 2021–2038. https://doi.org/10.1029/2018JG004712

Hobbie, J. E., & Kling, G. W. (Eds) (2014). *Alaska's changing Arctic: Ecological consequences for tundra, streams, and lakes*. Oxford, UK: Oxford University Press. https://doi.org/10.1093/acprof:osobl/9780199860401.001.0001

Kana, T. M., Darkangelo, C., Hunt, M. D., Oldham, J. B., Bennett, G. E., & Cornwell, J. C. (1994). Membrane inlet mass spectrometer for rapid high-precision determination of N2, O2, and Ar in environmental water samples. *Analytical Chemistry*, *66*(23), 4166–4170. https://doi.org/10.1021/ac00095a009

Longworth, B. E., von Reden, K. F., Long, P., & Roberts, M. L. (2015). A high output, large acceptance injector for the NOSAMS Tandetron AMS system. *Nuclear Instruments and Methods in Physics Research B*, *361*, 211–216. https://doi.org/10.1016/j.nimb.2015.04.005

Mangiante, D. M., Schaller, R. D., Zarzycki, P., Banfield, J. F., & Gilbert, B. (2017). Mechanism of ferric oxalate photolysis. *ACS Earth and Space Chemistry*, *1*(5), 270–276. https://doi.org/10.1021/acsearthspacechem.7b00026

McGuire, A. D., Lawrence, D. M., Koven, C., Clein, J. S., Burke, E., Chen, G., et al. (2018). Dependence of the evolution of carbon dynamics in the northern permafrost region on the trajectory of climate change. *Proceedings of the National Academy of Sciences of the United States of America*, *115*(15), 3882–3887. https://doi.org/10.1073/pnas.1719903115

McNichol, A. P., Jones, G. A., Hutton, D. L., & Gagon, A. R. (1994). The rapid preparation of seawater ΣCO_2 for radiocarbon analysis at the National Ocean Sciences AMS facility. *Radiocarbon*, *36*(2), 237–246. https://doi.org/10.1017/S0033822200040522

McNichol, A. P., Jull, A. J. T., & Burr, G. S. (2001). Converting AMS data to radiocarbon values: Considerations and conventions. *Radiocarbon*, *43*(2A), 313–320. https://doi.org/10.1017/S0033822200038169

Miles, C., & Brezonik, P. (1981). Oxygen consumption in humic-colored waters by a photochemical ferrous-ferric catalytic cycle. *Environmental Science & Technology*, *15*(9), 1089–1095. https://doi.org/10.1021/es00091a010

Miller, C. J., Rose, A. L., & Waite, T. D. (2009). Impact of natural organic matter on H_2O_2-mediated oxidation of Fe(II) in a simulated freshwater system. *Geochimica et Cosmochimica Acta*, *73*(10), 2758–2768. https://doi.org/10.1016/j.gca.2009.02.027

Mull, C. G., & Adams, K. E. (Eds) (1989). *Bedrock geology of the eastern Koyukuk Basin, central Brooks Range, and east central Arctic Slope along the Dalton Highway, Yukon River to Prudhoe Bay, Alaska Guidebook 7*, (Vol. 1). Anchorage, AK: Department of Natural Resources, Division of Geological and Geophysical Surveys.

Ping, C. L., Bockheim, J. G., Kimble, J. M., Michaelson, G. J., & Walker, D. A. (1998). Characteristics of cryogenic soils along a latitudinal transect in Arctic Alaska. *Journal of Geophysical Research*, *103*(D22), 28,917–28,928. https://doi.org/10.1029/98JD02024

Plaza, C., Pegoraro, E., Bracho, R., Celis, G., Crummer, K. G., Hutchings, J. A., et al. (2019). Direct observation of permafrost degradation and rapid soil carbon loss in tundra. *Nature Geoscience*, *12*(8), 627–631. https://doi.org/10.1038/s41561-019-0387-6

Schuur, E. A. G., McGuire, A. D., Schädel, C., Grosse, G., Harden, J. W., Hayes, D. J., et al. (2015). Climate change and the permafrost carbon feedback. *Nature*, *520*(7546), 171–179. https://doi.org/10.1038/nature14338

Selvam, B. P., Lapierre, J. F., Guillemette, F., Voigt, C., Lamprecht, R. E., Biasi, C., et al. (2017). Degradation potentials of dissolved organic carbon (DOC) from thawed permafrost peat. *Nature Scientific Reports*, *7*(1), 45,811. https://doi.org/10.1038/srep45811

Shirokova, L. S., Chupakov, A. V., Zabelina, S. A., Neverova, N. V., Payandi-Rolland, D., Causseraund, C., et al. (2019). Humic surface waters of frozen peat bogs (permafrost zone) are highly resistant to bio- and photodegradation. *Biogeosciences*, *16*(12), 2511–2526. https://doi.org/10.5194/bg-16-2511-2019

Šmejkalová, T., Edwards, M. E., & Dash, J. (2016). Arctic lakes show strong decadal trends in earlier spring ice-out. *Nature Scientific Reports*, *6*(1), 38,449. https://doi.org/10.1038/srep38449

Spencer, R. G. M., Stubbins, A., Hernes, P. J., Baker, A., Mopper, K., Aufdenkampe, A. K., et al. (2009). Photochemical degradation of dissolved organic matter and dissolved lignin phenols from the Congo River. *Journal of Geophysical Research*, *114*, G03010. https://doi.org/10.1029/2009JG000968

Stubbins, A., Mann, P. J., Powers, L., Bittar, T. B., Dittmar, T., McIntyre, C. P., et al. (2016). Low photolability of yedoma permafrost dissolved organic carbon. *Journal of Geophysical Research: Biogeosciences*, *122*, 200–211. https://doi.org/10.1002/2016JG003688

Stuiver, M., & Polach, H. A. (1977). Discussion: Reporting of ^{14}C data. *Radiocarbon*, *19*(3), 355–363. https://doi.org/10.1017/S0033822200003672

Trusiak, A., Treibergs, L. A., Kling, G. W., & Cory, R. M. (2019). The controls of iron and oxygen on hydroxyl radical (•OH) production in soils. *Soil System*, *3*(1), 1. https://doi.org/10.3390/soilsystems3010001

Walker, D. A., Raynolds, M. K., Daniëls, F. J. A., Einarsson, E., Elvebakk, A., Gould, W. A., et al. (2005). The circumpolar Arctic vegetation map. *Journal of Vegetation Science*, *16*(3), 267–282. https://doi.org/10.1111/j.1654-1103.2005.tb02365.x

Ward, C. P., Armstrong, C. J., Walsh, A. N., Jackson, J. J., & Reddy, C. M. (2019). Sunlight converts polystyrene into carbon dioxide and dissolved organic carbon. *Environmental Science & Technology Letters*, *6*(11), 669–674. https://doi.org/10.1021/acs.estlett.9b00532

Ward, C. P., & Cory, R. M. (2016). Complete and partial photo-oxidation of dissolved organic matter draining permafrost soils. *Environmental Science & Technology*, *50*(7), 3545–3553. https://doi.org/10.1021/acs.est.5b05354

Ward, C. P., Nalven, S. G., Crump, B. C., Kling, G. W., & Cory, R. M. (2017). Photochemical alteration of organic carbon draining permafrost soils shifts microbial metabolic pathways and stimulates respiration. *Nature Communications*, *8*(1), 772–778. https://doi.org/10.1038/s41467-017-00759-2

Xie, H., Zafiriou, O. C., Cai, W. -J., Zepp, R. G., & Wang, Y. (2004). Photooxidation and its effects on the carboxyl content of dissolved organic matter in two coastal rivers in the southeastern United States. *Environmental Science & Technology*, *38*(15), 4113–4119. https://doi.org/10.1021/es035407t